View metadata, citation and similar papers at core.ac.uk

brought to you by CORE

provided by Open Archive Toulouse Archive

Open Archive Toulouse Archive Ouverte (OATAO)

OATAO is an open access repository that collects the work of Toulouse researchers and makes it freely available over the web where possible.

This is an author-deposited version published in: http://oatao.univ-toulouse.fr/
Eprints ID: 3743

To link to this article: DOI:10.1016/j.matchar.2009.04.007
URL: http://dx.doi.org/10.1016/j.matchar.2009.04.007

To cite this version: Voicu, Raluca and Andrieu, Eric and Poquillon, Dominique and Furtado, Jader and Lacaze, Jacques (2009) *Microstructure evolution of HP40-Nb alloys during aging under air at 1000 °C.* Materials Characterization, 60 (9). pp. 1020-1027. ISSN 1044-5803

Any correspondence concerning this service should be sent to the repository administrator: staff-oatao@inp-toulouse.fr

Microstructure evolution of HP40-Nb alloys during aging under air at 1000 °C

Raluca Voicu[a], *Eric Andrieu*[a], *Dominique Poquillon*[a], *Jader Furtado*[b], *Jacques Lacaze*[a,*]

[a]*Université de Toulouse, CIRIMAT, ENSIACET, 118 route de Narbonne, 31077 Toulouse Cedex 04, France*
[b]*Air Liquide, C.R.C.D, 1 chemin de la Porte des Loges, Les Loges-en-Josas, 78354 Jouy-en-Josas Cedex, France*

Article history:
Received 26 January 2009
Received in revised form
27 March 2009
Accepted 6 April 2009

Keywords:
HP alloy
Heat resistant steel
Carbo-nitrides
Carbides

A B S T R A C T

Two as-cast HP 40 alloys provided by different manufacturers were aged at 1000 °C under laboratory air. They had the same as-cast microstructure consisting of austenite dendrites delineated by a network of eutectic Nb-rich MC and Cr-rich M_7C_3 carbides. After aging for several months, they showed similar microstructures in the bulk materials, though M_7C_3 carbides have been replaced by $M_{23}C_6$ carbides. As expected, a sub-surface zone depleted in chromium has appeared where a tetragonal CrNbC could be identified in both materials. However, the composition of the transition zones between the surface and the bulk materials differed, mainly because one of the materials underwent significant nitrogen pick-up with associated precipitation of M_6(C,N) and M_2(C,N) phases. On the contrary, the other alloy did show only one intermediate zone with a mix of CrNbC, $M_{23}C_6$ and MC carbides. A full account of the microstructures observed in the aged materials is given.

1. Introduction

Cast austenitic stainless steels of the H-series are commonly used as reformer tubes working at temperatures that can be close to 1000 °C. This work reports results obtained as part of a study devoted to a better understanding of the various factors affecting life-time of such reformer tubes, e.g. service temperature, environment, microstructure aging and thermo-mechanical loadings. In a parallel study, the corrosion behaviour of two HP-40 heat resisting austenitic steels in $CO+CO_2$ gas mixtures was studied [1]. The present work focuses on microstructure evolution of these two materials during aging at 1000 °C for 3, 6 and 9 months under laboratory air in order to have reference microstructures for further investigations.

2. Experimental Details

The two materials will be denoted A and B, they were labeled respectively A1 and A2 by Xu et al. [1]. They were provided as cylindrical pieces of tubes that were 26 mm in thickness and 138 mm in outer diameter for material A, 15 mm in thickness and 138 mm in outer diameter for material B. Samples encompassing the whole section thickness were machined out from each tube and were heat-treated under laboratory air for 3, 6 and 9 months at 1000 °C. All observations and characterizations have been performed on plane sections through the thickness of the tubes.

The as-cast macrostructure was first observed by optical microscopy that allowed visualizing the grain distribution after appropriate etching with Behara BII (48 g NH_4F-HF, 800 ml H_2O, 400 ml HCl) of mirror polished specimens as illustrated in Fig. 1. It is seen that the thinner tube A presents only a radial columnar structure while the thicker B one exhibits an outer columnar zone (16 mm thick) and an inner equiaxe zone.

After repolishing of the as-cast samples, energy dispersive spectrometry (EDS) analyses through the tube thickness have been carried out to: i) check the presence of any macroscopic chemical heterogeneity; and ii) estimate the average composition of the alloys. These analyses were performed by scanning over $450\times340\ \mu m^2$ windows (i.e. about 0.15 mm^2) on a scanning

* *Corresponding author.*
E-mail address: jacques.lacaze@ensiacet.fr (J. Lacaze).

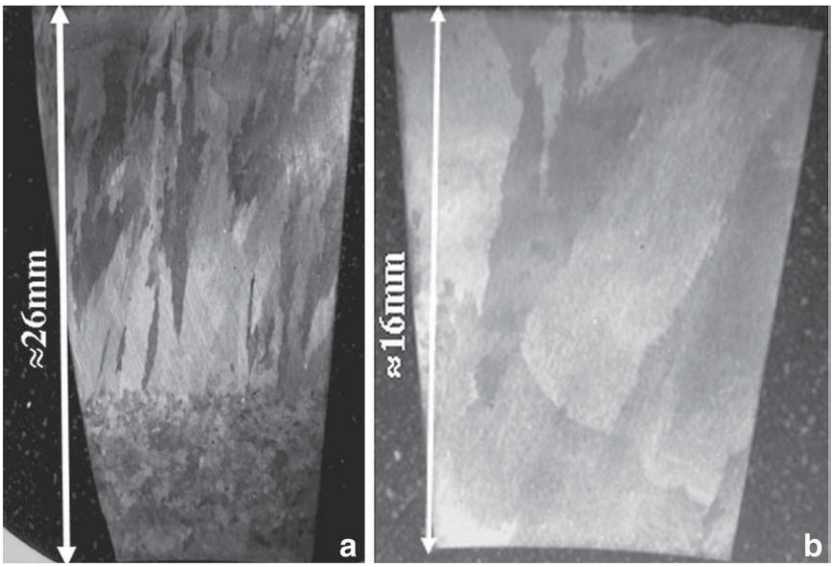

Fig. 1 – Optical macrographs through the tube thickness of materials A (a) and B (b).

electron microscope (SEM). These windows were implemented jointly through the sections, and X-ray acquisition was carried out during 200 s on each. Counts of the elements listed in Table 1 and of carbon and nitrogen were then processed by means of a Phi-Rho-Z correction method. While the "goodness of fit" of the measurements, i.e. the quality of the recorded spectra, was always good, the sum of the true contents after correction was not always close to the expected 100 wt.% so that the data was then normalized for further use. As the carbon and nitrogen contents cannot be determined quantitatively by EDS, though semi-quantitative variations will be considered later in this paper, the normalization was made on the metallic species using the following formula:

$$w_i^{cor} = 100 \cdot \frac{w_i}{\sum_i w_i - w_C - w_N}$$

where w_i is the true content in i species after Phi-Rho-Z calculation and w_i^{cor} is the i content after normalization.

Also, Table 1 gives the theoretical standard deviation for each species for a composition typical of the EDS analyses made. It is seen that for all elements but Fe, Ni and Cr, the standard deviation is very high, being in some cases even larger than the estimated content. For low level alloying elements, additional chemical analyses have been performed using glow discharge mass spectrometry (GDMS) and combustion analysis (for C and S).

Characterization of the phases present in as-cast and heat-treated materials were realized by spot counting with EDS in the SEM with an acquisition time of 100 s. The raw data were processed as described above to give the true species contents. In addition, a few electron probe micro-analysis (EPMA) analyses have been also performed on specimens polished down to 1/4 μm. A focused spot was used so that the analyzed volume is a few μm^3, and counting was carried out during 20 s. This technique allowed semi-quantitative evaluation of interstitial elements (C and N) together with quantitative analysis of other elements. True weight fractions were obtained by ZAF correction and no normalization was performed in that case.

Chemical characterizations have been complemented with X-ray diffraction analyses (XRD) carried out on samples polished down to 2400 SiC paper. The X-ray beam was positioned close to the middle of the section of the tube and XRD patterns were recorded in the 2θ range 34–47° using the Cu-K_α radiation ($\lambda_{K\alpha1}$=1.541 Å). Reflections were collected by step scanning with 2q intervals of 0.05° and counting time of 60 s for each step.

Finally, thin foils were prepared for transmission electron microscopy (TEM) analysis of A and B materials heat-treated for 9 months. The thin foils were obtained from a mounting of two parallelepipeds cut off from the internal surface of the tubes with the two surfaces facing each other. The two parallelepipeds were then introduced in a 3 mm diameter brass tube and glued with an epoxy resin. After drying, 300 μm thick discs were sectioned from the tube that were afterwards mechanically polished down to about 100 μm, dimpled and finally thinned by Ar ion-milling using a precision ion polishing system (PIPS) until a hole was detected. Care was taken all along the preparation that these holes encompass the oxidized surface of the tube and go as far as possible inside the bulk material. Holes penetrating 300 μm deep in the

Table 1 – Typical EDS analysis and theoretical standard deviation (wt.%) related to each species considered during EDS analysis of HP40 alloy.

	Fe	Ni	Cr	Nb	Si	Al	Ta	Mg	Mo	Mn	W	Ti	V
Composition	37.2	32.6	25.5	1.0	1.5	0.1	0.2	0.1	0.1	1.3	0.4	0.2	0.1
Standard deviation	0.9	1.0	0.6	0.3	0.2	0.4	0.2	0.6	0.15	0.2	0.3	0.5	0.2

Table 2 – Chemical composition of the as-cast materials as obtained by SEM-EDS analysis for most elements, GDMS for Al and Ti, and combustion for C and S.

	Ni	Cr	Nb	Si	Al	Ta	Mo	Mn	W	Ti	C	S
A	32.6	25.5	1	1.5	8.2	0.2	0.1	1.3	0.4	340	0.42	120
B	34.9	26	1	1	560	0.2	0.1	0.7	1	1400	0.43	41

Values are given in wt.% except for Al, Ti and S that are in ppm per weight.

sample were thus obtained. TEM observations were carried out at 200 kV.

3. Results

3.1. *As-Cast Materials*

The overall chemical analyses obtained by EDS for major elements, GDMS or combustion for low level elements, are given in Table 2. They do agree fairly exactly with those reported for the same tubes by Xu et al. [1] though these authors did not report any value for Mg and V that were also detected in the present work. The only discrepancy is in the Nb content of material B, 1 wt.% in Table 1 as compared to 1.4 wt.% according to Xu et al. [1]. It should be noted that the compositions of materials A and B show significant differences

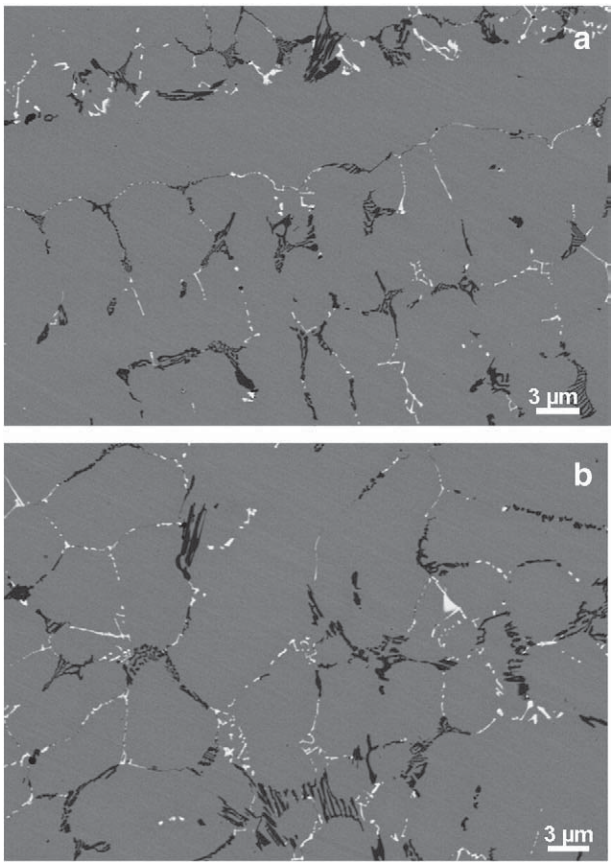

Fig. 2 – QBSD images on A material (a: columnar zone, b: equiaxe zone).

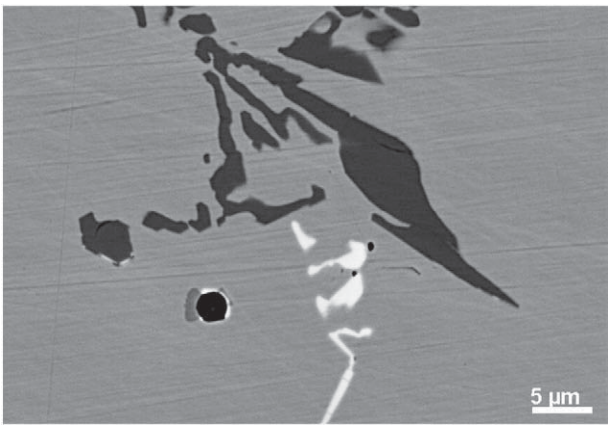

Fig. 3 – Micrograph of as-cast A material at high enlargement.

for some of the minor elements that affect oxidation, namely Al, Si, Mn and Ti.

The SEM micrographs in Fig. 2 illustrate the as-cast microstructure observed with the quadrant back scattered detection (QBSD) mode in the columnar and equiaxe zones of tube A. At this enlargement, the austenite dendrites are evidenced by a network of precipitates in alternating white and dark contrast. The micrograph taken in the columnar zone is also representative of what was observed on the B material. A fine precipitation could be observed in the matrix in the outer zone of tube A that was not seen in other locations of this material and in any location of tube B.

Higher magnification images were recorded as illustrated in Fig. 3 and coupled with EDS analysis. In these, the presence of carbon was checked though not quantified. When this latter species was present at a high level, the phase could be identified as a carbide. Precipitates in white contrast correspond to Nb-rich carbides whereas most black precipitates correspond to Cr-rich carbides. Some rare manganese sulfides with a rounded shape as well as titanium oxides and titanium–niobium precipitates with cubical shapes were also observed, which all have a dark contrast. Individual EDS analyses of the two major phases gave very similar compositions for precipitates with identical contrast, which could then be grouped together and tentatively associated to a single phase. Accordingly, the contrast on QBSD images and the average compositions of these two phases are given in Table 3. Mg and V were not found at any significant level in either of the precipitates and thus have not been listed.

Table 3 – QBSD contrast and composition (wt.%) of the two phases observed in A and B tubes.

	Contrast	Al	Cr	Fe	Mn	Mo	Nb	Ni	Si	Ta	Ti	W
A	White	ε	6.7	4.4	0.1	0.1	81.8	3.9	0	0	2.1	0.3
	Black	0.1	86.8	10.2	0.4	0	0.4	1.4	0	ε	0	0.1
B	White	0	5.0	2.9	ε	ε	82.0	2.7	0	0	5.2	1.4
	Black	ε	86.7	8.7	0.3	ε	0.4	1.5	0	0.4	ε	1.3

0 and ε are respectively for no traces and traces of the related element.

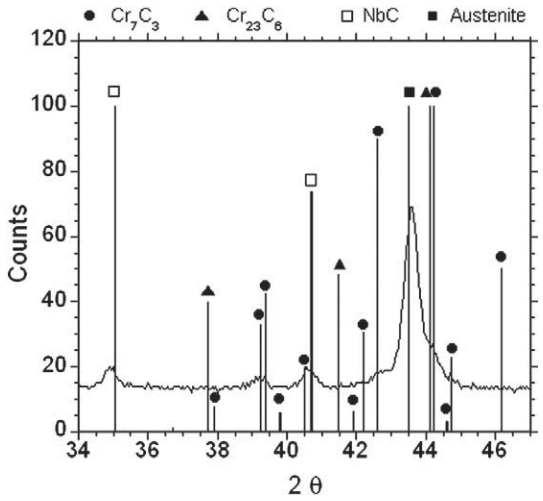

Fig. 4 – XRD pattern recorded on A as-cast material.

X-ray diffraction patterns were recorded on both as-cast materials that appeared to give exactly the same features. In the one relative to material A that is shown in Fig. 4, it is seen that two carbides, namely MC and M_7C_3, are present. According to the compositions showed in Table 3, it may be concluded that MC and M_7C_3 carbides appear respectively in white and dark contrast on the QBSD micrographs.

3.2. *Laboratory-Aged Materials*

Figs. 5 and 6 illustrate the evolution of the microstructure of materials A and B observed from the surface to the bulk of the section after 6 months aging at 1000 °C. From SEM observation, four zones could be defined from the surface to the centre in material A, whenever the outer or inner surface of the tube was considered. Analysis of these zones as detailed below led to define them as: an outer zone depleted in chromium (Cr-DZ), an outer intermediate zone (OIZ) and an inner intermediate zone (IIZ) that both contain carbo-nitrides, and finally the bulk material (bulk). In Fig. 6, it is seen that material B did show only three zones, a Cr-depleted zone (Cr-DZ), one single intermediate zone (IZ) and the bulk material (bulk). As for material A, these features were the same from either the outer or the inner surfaces of material B.

As a matter of fact, the aging time did not lead to significant changes in the size and features of the intermediate zones that presented similar microstructure after 3, 6 or 9 months aging. Most of the results presented below are related to 6 months aging.

3.3. *Bulk Materials*

The observation of the microstructure in the bulk of both materials, as illustrated in Figs. 5 and 6, showed that the primary

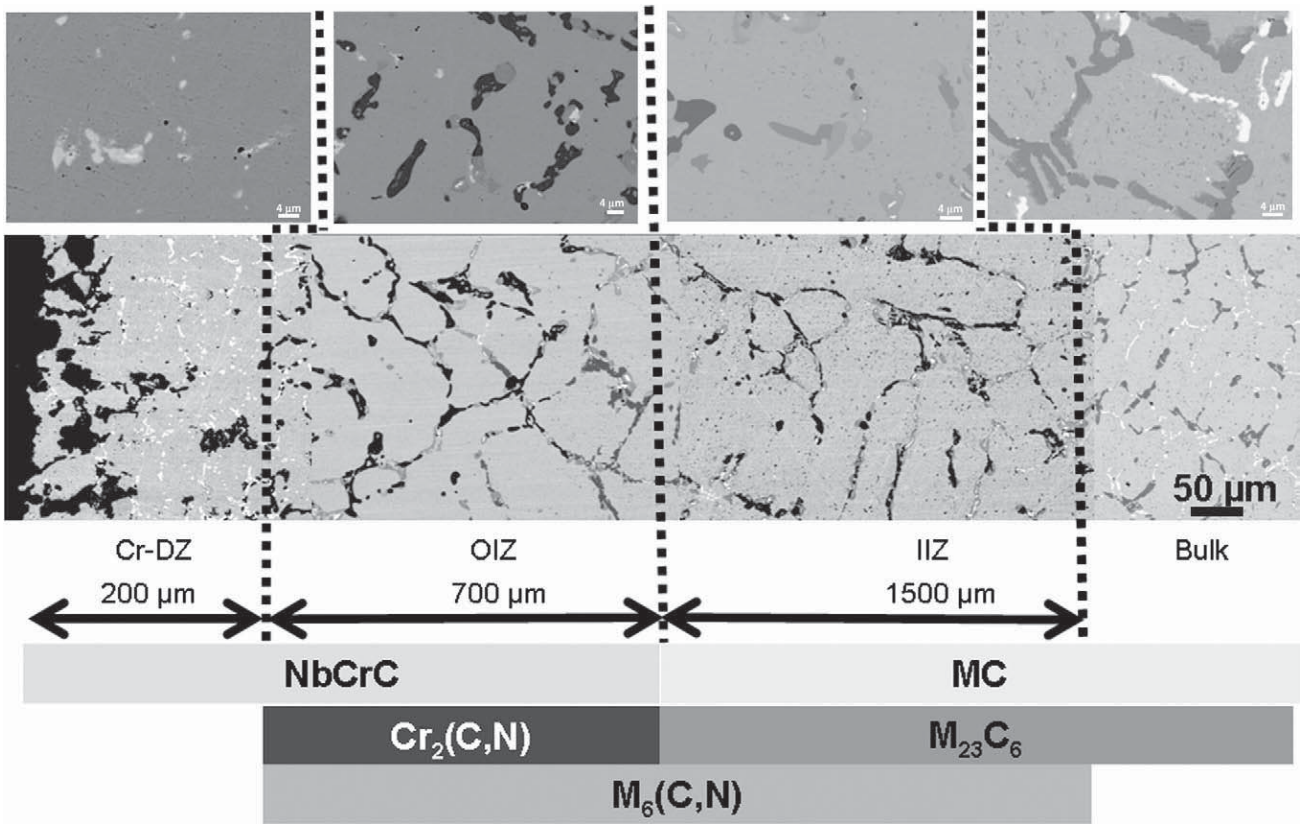

Fig. 5 – SEM images of the different zones from inner surface in A material aged 6 months and corresponding schematic of the phases present. The upper row shows micrographs at higher enlargement than in the bottom row for each of the four zones identified.

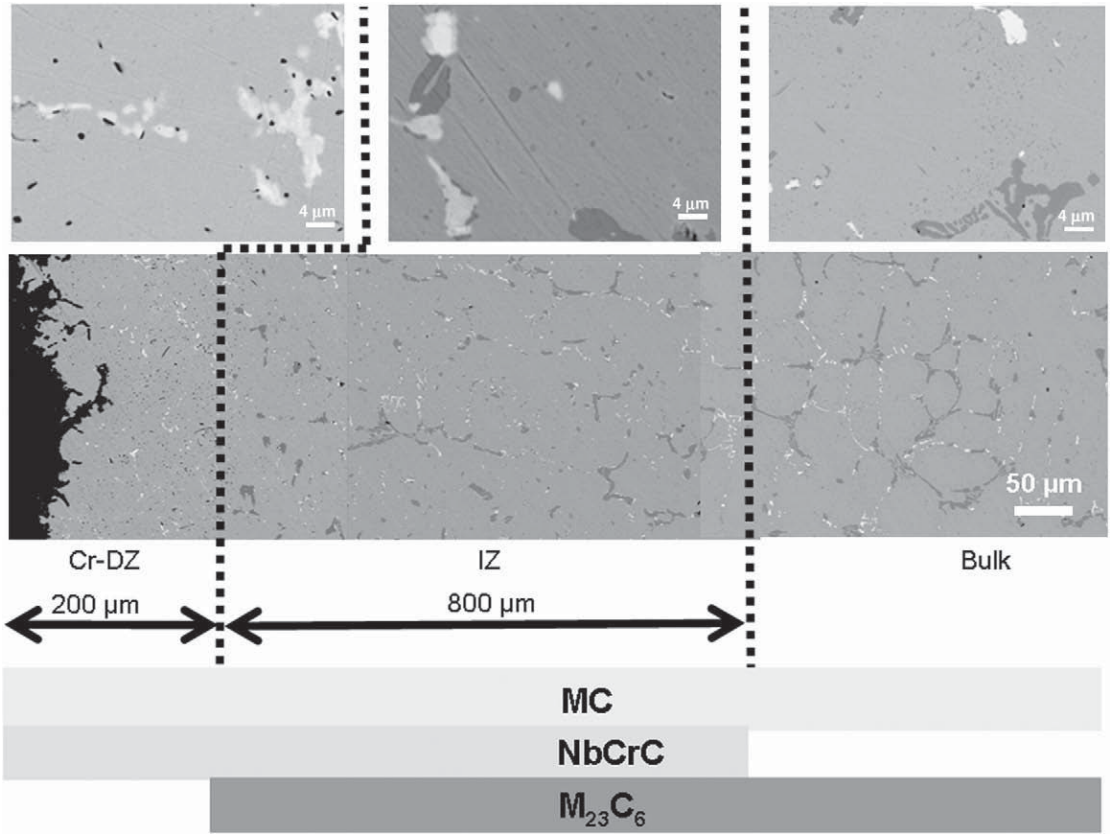

Fig. 6 – SEM images of the different zones from inner surface in B material aged 6 months and corresponding sketch of the phases present. The upper row shows micrographs at higher enlargement than in the bottom row for each of the three zones identified.

chromium-rich precipitates (grey contrast) have coarsened during aging. As expected from literature [2,3], it has been verified by XRD that the initial M_7C_3 carbides have transformed into $M_{23}C_6$. Precipitates in white contrast that correspond to Nb-rich MC carbides remained unaltered with aging, except for some coarsening. A secondary precipitation of chromium-rich carbides was observed within the matrix, which appears slightly coarser in material A than in material B. To ascertain that this secondary precipitation took place during aging and not during cooling of the samples at the end of the heat treatment, an aged sample was reheated at 1000 °C during 15 min and water quenched. The secondary precipitation was still observed on this sample, thus ascertaining it appeared as a result of aging. Though the size of these precipitates is rather small for accurate EDS analysis, they appeared to be rich in chromium and were thus assumed to be $M_{23}C_6$.

3.4. *Chromium-Depleted Zone*

Along the surface of both aged materials, a zone of 150 to 200 µm thick with light grey and dark precipitates was noticed. X-ray maps were acquired by EDS at the magnification ×200 as illustrated in Fig. 7 for Cr and Si in the case of material A. It is seen that this zone corresponds to a Cr-depleted zone, and a parallel depletion in Mn could also be evidenced. This is due to outward diffusion of Cr and Mn that relates to the development of the outer scale made of Cr-rich and Mn-rich oxides [1]. Internal oxidation of silicon occurs that is associated to simultaneous Si depletion in the matrix and Si accumulation at grain boundaries and along the oxide scale as reported by Xu et al. [1]. The comparison of the EDS maps with the QBSD image in Fig. 7 shows that the dark precipitates in the Cr-DZ zone are rich in silicon, thus certainly consisting in silica. The precipitates in light contrast were found to contain some carbon and to be rich in Nb and Cr, with an average composition close to Nb55Cr35Ti5Fe3Ni1 (wt.%). A close examination of these precipitates, illustrated with the micrograph at high enlargement in Fig. 5, showed in some cases small white particles embedded in them that are certainly remains of the previous Nb-rich MC carbide. It seems that the amount of residual MC carbide was slightly larger in material B (see the corresponding enlarged micrograph in Fig. 6).

TEM observations of A and B materials performed on the first 100 µm from the surface, i.e. corresponding to Cr-DZ zone, confirmed the presence of tetragonal SiO_2 (a=4.978 Å and c=6.9480 Å). In B material and not in the A one, small precipitates of alumina and of a phase rich in niobium and titanium were observed up to 200 µm inwards, i.e. at the inner boundary of the Cr-DZ zone. This latter phase could be identified as MC carbide with a Fm3m space group and a lattice parameter of about 4.469 Å. Finally, micrometric precipitates rich in Nb and Cr were observed on both A and B laboratory aged alloys that were found using diffraction patterns to be identical to the CrNbN phase with a tetragonal structure (P4bm space group, a=3.037 Å and c=7.391 Å) [4]. While its chemical formula is very close to the one of the Z

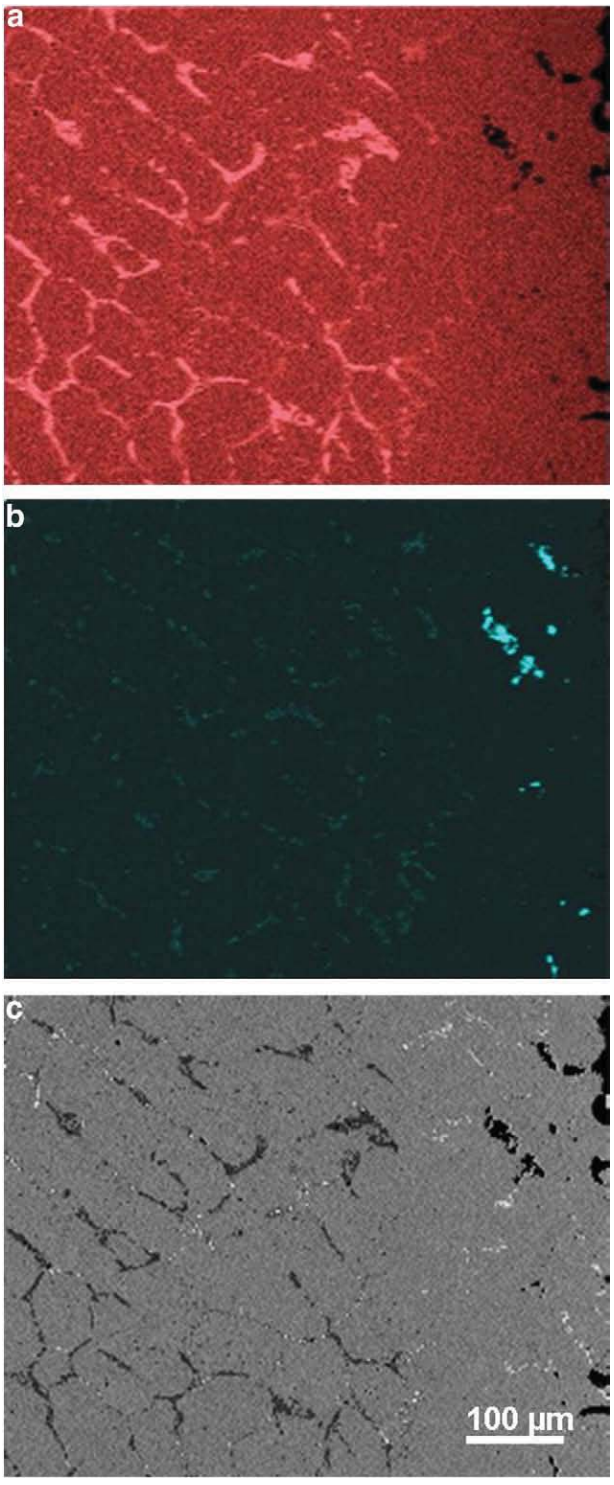

Fig. 7 – X-ray maps of Cr (a) and Si (b), and QBSD micrograph (c) in the inner zone of the A material aged 3 months.

phase that is often observed after aging steels stabilized with Nb [5,6], the space groups differ as it is P4/nmm for the Z phase. This suggests that the phase labeled Nb55Cr35Ti5-Fe3Ni1 above is in fact the CrNbC variant of the tetragonal CrNbN phase. Note that additional EPMA analysis of this phase confirmed the presence of carbon while no nitrogen was detected.

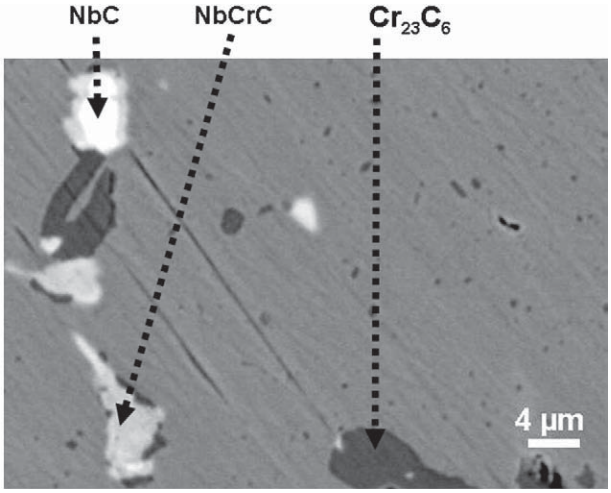

Fig. 8 – Precipitates in the intermediate zone of the aged B material.

3.5. *Intermediate Zones*

The enlarged micrograph for the IZ zone of material B in Fig. 6 shows that there are three different phases in addition to austenite. The micrograph has been reproduced in Fig. 8 where the phases identified through SEM and TEM examination are labelled. It is seen that this zone consists in a transition from the bulk material with MC and $M_{23}C_6$ precipitates to the sub-surface zone where only CrNbC phase and residues of MC were observed.

In contradistinction with this somehow simple transition scheme observed in material B, material A presents two intermediate zones, OIZ and IIZ in Fig. 5. The outer intermediate zone OIZ is about 600–700 µm thick with a microstructure illustrated with the micrograph in Fig. 9. In addition to some traces of Nb-rich MC and to precipitates of the CrNbC phase, two types of carbo-nitrides were identified: i) a Cr-rich carbo-nitride that appears with a dark contrast and a lacy shape that will be labelled as (C,N)Cr; and ii) a light-grey carbo-

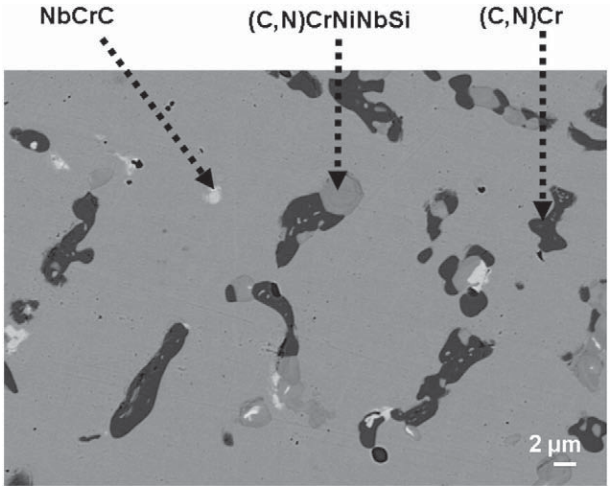

Fig. 9 – SEM micrograph of the OIZ intermediate zone of aged A material. Light-grey contrast: NbCrC, grey contrast: M_6(C, N), dark grey contrast: Cr_2(C, N).

Table 4 – Range of composition (wt.%) of the phases identified in A and B as-cast and laboratory aged materials as measured by SEM-EDS (normal font) and by EPMA (bold italics).

		Fe	Ni	Cr	Nb	Ti	W	C	N	Si
MC	A as-cast	1–9	1–9	3–9	70–90	1–10				
	A aged	1–2	2–4	3–7	84–92	2–3	1–2			
	B as-cast	1–5	1–5	3–7	77–85	3–9				
	B aged	1–4	1–3	3–15	72–87	3–15	1–5			
M_7C_3	A as-cast	10–11	1–2	86–87	1					
	B as-cast	8–9	1–2	85–89	0–1					
$M_{23}C_6$	A aged	11–14	4–5	79–83						
	B aged	9–10	4–5	80–83			2–4			
NbCrC	A aged	4–8	1–4	34–42	51–58	0–3				
	B aged	2–12	1–2	26–38	52–60	3–7				
$M_6(C,N)$	A aged	3–4	31–33	36–42	7–14		0–1			6–10
		3.6–6.8	*30–33*	*33–43*	*6.5–14.8*			*0.7–2*	*1.7–2*	*4.9–8*
$Cr_2(C,N)$	A aged	2–3	0–1	87–92	0–1					
		7.6–10	*7–17*	*60–70*	*2.4–5.8*			*1.5–3.6*	*1–1.8*	*1–3.7*

nitride containing Cr, Ni, Nb and Si, labelled (C,N)CrNiNbSi. EPMA analyses were performed on this sample that allowed a more precise quantification of interstitial elements and showed this latter phase to contain about 2 wt.% N.

In the OIZ zone of material A, TEM analysis allowed identification of Cr-rich precipitates as Cr_2N with a hexagonal structure (space group P3 1 m, lattice parameters a=4.75 Å and c=4.44 Å). The formula of these precipitates should be rather $Cr_2(C,N)$ since EPMA analysis confirmed the presence of both carbon and nitrogen. The other precipitates that are rich in Ni and Cr, and contain niobium and silicon as well, could be identified as M_6C with a cubic structure (space group Fd3m, a=10.6 Å). EPMA showed them to contain both nitrogen and carbon, so that the phase corresponds to $M_6(C,N)$ carbo-nitride and could be written $M_5Si(C,N)$ [7,8].

The transition from the OIZ zone to the IIZ zone towards the bulk of the material is sharply marked with the appearance of a secondary precipitation, the disappearance of black chromium-rich precipitates (C,N)Cr and the appearance of $M_{23}C_6$. Assuming that secondary precipitates are $M_{23}C_6$ as in the bulk material, the IIZ zone contains three phases MC, $M_{23}C_6$ and $M_6(C,N)$. The schematics at the bottom of Figs. 5 and 6 summarize the phases observed in the various zones identified in materials A and B after aging, while Table 4 lists the range of composition of all the phases as evaluated by EDS and EPMA. It is seen that $M_6(C,N)$ can be easily differentiated from other phases thanks to its high level of Si. Note that the $Cr_2(C,N)$ phase has a composition in metallic elements that makes it quite similar to $M_{23}C_6$.

4. Discussion

Though no detailed study of the oxide scales was performed during the present work, all the features observed are similar to those reported by Xu et al. [1]. The outer scale consists of chromium-rich and manganese-rich oxides, while internal oxidation involved silica that formed a more continuous layer in alloy B than in alloy A. This latter result appears surprising with respect to the relative silicon content of the alloys and could mot be explained [1]. Internal oxidation involves precipitation of other oxides [1], one rich in aluminium that was identified as alumina in the present work, and other precipitates rich in Ti and Nb.

In the bulk of both A and B materials, the transformation of M_7C_3 in $M_{23}C_6$ is in agreement with literature [2,7,8], though no precipitate of G phase was observed. This may be due to the aging temperature that appears to be in the upper range for the formation of this phase [2], and also to the low level of Nb [2,9,10] and Si [11] of the investigated alloys. In the chromium depleted zone, the present results show that Nb-rich MC carbides have transformed to NbCrC carbides, either nearly totally for alloy A or partly for alloy B. This transformation was not mentioned by Xu et al. [1] and appears triggered by the dissolution of the Cr-rich $M_{23}C_6$ precipitates as clearly evidenced by the observation of the intermediate zone in alloy B. Though such a phase was not found in the study of the liquidus of the C–Cr–Nb phase diagram [12], a tetragagonal (P4bm) NbCr(C,N) phase has been observed by Yong-Jun Oh et al. [13] in steels doped with various amounts of C and N.

Due to the fact that alloys A and B have very close compositions it is not expected that thermodynamics could explain nitrogen pick-up in alloy A and not in alloy B. It is thus suggested that the nearly continuous silica layer formed at the oxide/metal interface of the B materials did protect it against nitrogen penetration. If this assumption applies, it should be expected that carbon released by dissolution of $M_{23}C_6$ precipitates would hardly leave the material during heat-treating of B material while it could in the case of alloy A. Accordingly, the carbon content in the bulk of the material should increase in case of alloy B. Table 5 shows the results of carbon content analysis performed by combustion analysis on specimens machined out from the central part of as-cast material and samples aged 9 months. To improve the reliability of these measurements, they have been done altogether at the

Table 5 – Carbon content in bulk alloys A and B in the as-cast state and after heat-treating 9 months.

	A as-cast	A heat-treated	B as-cast	B heat-treated
Carbon content (wt.%)	0.40	0.42	0.41	0.47

AZTERLAN research centre, the standard deviation on each analysis being 0.01 wt.% C. It is clearly seen that there is a significant increase of the carbon content in the bulk of material B after aging that sustains the above assumption.

It is anyway surprising that so few works did report the formation of nitrides or carbo-nitrides in cast austenitic steels. The only work is due to Powell et al. [14] that observed a partial substitution of carbon by nitrogen in the $M_{23}C_6$ phase of 20–25 steels that was related with the parallel transformation of MC to G phase.

5. Conclusion

The two commercial HP40Nb grade alloys presently studied were found to exhibit different microstructure evolutions during aging under air at 1000 °C, although the bulk materials and the outer chromium depleted zones showed the same phases. These differences are related to nitrogen pick-up for one of the material while the other appeared free of that phenomenon. In the alloy without nitrogen pick-up, chromium depletion due to growth of the outer scale led to decomposition of $M_{23}C_6$ carbides that triggers the transformation of Nb-rich carbides in CrNbC carbides. This latter phase is tetragonal and was previously referenced as CrNbN phase, though it has also been found it could be a carbo-nitride. In the alloy that was prone to nitrogen pick-up, the transformation path is more complicated with the successive formation of two carbo-nitrides, M_6(C,N) and then Cr_2(C,N) in addition to the CrNbC carbide. This difference between the two investigated materials was tentatively related to the fact that, in spite of their close chemical compositions, the alloys showed slight changes in the inner oxide scale. The alloy that did not pick-up nitrogen developed a continuous silica layer that may have protected it against nitrogen diffusion, while in the other alloy silicon was associated with internal oxidation. The capability of the continuous silica layer against nitrogen pick-up should also protect against carbon loss as effectively observed, and this sustains the proposed explanation for the different transformation paths showed by the alloys.

Acknowledgements

Thanks are due to P. de Parceval for EPMA analyses performed at the “service commun d’analyse” in Toulouse, to M.-C. Lafont for TEM observations made at TEMSCAN (Université Paul Sabatier in Toulouse, France) and S. Mendes for the carbon analyses performed in the Metallurgy Research centre of AZTERLAN (Durango, Spain).

REFERENCES

[1] Xu N, Monceau D, Young D, Furtado J. High temperature corrosion of cast heat resisting steels in Co + CO_2 gas mixtures. Corr Sci 2008;50:2398–406.
[2] Almeida Soares GD, Almeida LH, Silveira TL, May IL. Niobium additions in HP heat-resistant cast stainless steels. Mater Charact 1992;29:387–96.
[3] Wang F, Northwood DO. The effect of carbon content on the microstructure of an experimental heat-resistant steel. Mater Charact 1993;31:3–10.
[4] Villars P. Pearson’s Handbook. ASM International; 1997.
[5] Hughes H. Complex nitride in Cr–Ni–Nb steels. J Iron Steel Inst 1967;205:775–8.
[6] Jack DH, Jack KH. Structure of Z-phase, NbCrN. J Iron Steel Inst 1972;210:790–2.
[7] Padilha AF, Rios PR. Decomposition of austenite in austenitic stainless steels. ISIJ Int 2002;42:325–37.
[8] Sourmail T. Precipitation in creep resistant austenitic stainless steels. Mater Sci Technol 2001;17:1–14.
[9] Barbabela GD, Almeida LH, Silveira TL, May IL. Role of Nb in modifying the microstructure of heat-resistant cast HP steel. Mater Charact 1991;26:193–7.
[10] Barbabela GD, Almeida LH, Silveira TL, May IL. Phase characterization in two centrifugally cast HK stainless steel tubes. Mater Charact 1991;26:1–7.
[11] Ibanez RAP, Soares GDA, Almeida LH, May IL. Effects of Si content on the microstructure of modified-HP austenitic steels. Mater Charact 1993;30:243–9.
[12] Dovbenko OI, Bondar AA, Velikanova TY, Sleptsov SV. The (Cr) + (NbC) quasibinary eutectic in the Cr–Nb–C system. Powder Metall Met Ceram 2000;39:256–61.
[13] Oh Yong-Jun, Lee Byung Ju, Yoo One, Lee Bong Sang, Hong Jun Hwa. Precipitation behaviour of carbonitrides in type 347 stainless steels with various C and N contents. Metall Mater Trans A 2002;33A:1565–9.
[14] Powell DJ, Pilkington R, Miller DA. The precipitation characteristics of 20%Cr–25%Ni–Nb stabilized stainless steel. Acta Metall 1988;36:713–24.